Environ Earth Sci (2012) 67:549–561
DOI 10.1007/s12665-012-1703-2

SPECIAL ISSUE

Thermo-hydro-mechanical modeling of carbon dioxide injection for enhanced gas-recovery (CO_2-EGR): a benchmarking study for code comparison

Zhengmeng Hou · Yang Gou · Joshua Taron · Uwe Jens Gorke · Olaf Kolditz

Received: 2 January 2012 / Accepted: 19 April 2012 / Published online: 4 May 2012

Abstract The objective of this paper was to investigate the THM-coupled responses of the storage formation and caprock, induced by gas production, CO_2-EGR (enhanced gas recovery), and CO_2-storage. A generic 3D planer model (20,000 × 3,000 × 100 m, consisting of 1,200 m overburden, 100 m caprock, 200 m gas reservoir, and 1,500 m base rock) is adopted for the simulation process using the integrated code TOUGH2/EOS7C-FLAC3D and the multi-purpose simulator OpenGeoSys. Both simulators agree that the CO_2-EGR phase under a balanced injection rate (31,500 tons/year) will cause almost no change in the reservoir pressure. The gas recovery rate increases 1.4 % in the 5-year CO_2-EGR phase, and a better EGR effect could be achieved by increasing the distance between injection and production wells (e.g., 5.83 % for 5 km distance, instead of 1.2 km in this study). Under the considered conditions there is no evidence of plastic deformation and both reservoir and caprock behave elastically at all operation stages. The stress path could be predicted analytically and the results show that the isotropic and extensional stress regime will switch to the compressional stress regime, when the pore pressure rises to a specific level. Both simulators agree regarding modification of the reservoir stress state. With further CO_2-injection tension failure in reservoir could occur, but shear failure will never happen under these conditions. Using TOUGH-FLAC, a scenario case is also analyzed with the assumption that the reservoir is naturally fractured. The specific analysis shows that the maximal storage pressure is 13.6 MPa which is determined by the penetration criterion of the caprock.

Keywords CO_2-EGR · CO_2-storage · TOUGH-FLAC · OpenGeoSys · Thermo-hydro-mechanical modeling

Introduction

Carbon dioxide capture and storage (CCS) technologies are of significant global interest, being developed to reduce the emission of greenhouse gas (CO_2) into the atmosphere. It is recognized that most of the available geological storage capacity for CO_2 is in saline aquifers. However, CO_2 storage in oil and gas fields has many advantages. They are better characterized and have caprock seals that have successfully retained gas or oil for millions of years. The infrastructure is already in place and the computer model for the fields could be directly used to predict the movement of the gas (IEA 2004). Furthermore, CO_2 injection into depleted gas or oil fields can additionally enhance the gas or oil recovery (EOR/EGR).

While the CO_2-EOR technology has been developed and applied successfully over 40 years (IPCC 2005; Quintella et al. 2010; Sweatman et al. 2011), the CO_2-EGR

Z. Hou (✉)
Institute of Petroleum Engineering, Clausthal University of Technology, Agricolastr. 10, 38678 Clausthal-Zellerfeld, Germany
e-mail: hou@tu-clausthal.de

Z. Hou · Y. Gou
Energie-Forschungszentrum Niedersachsen, Goslar, Germany

Z. Hou · Y. Gou
Sino-German Energy Research Center, Sichuan University, Chengdu, China

J. Taron · U. J. Gorke · O. Kolditz
Helmholtz Center for Environmental Research, Leipzig, Germany

O. Kolditz
Technische Universität, Dresden, Germany

technology is relatively new and there are only a few CO_2-EGR demonstration projects in practice until now (Kühn et al. 2012; Martens et al. 2012). The reason is that the CO_2-EGR technology still has several unsolved problems, e.g., expensive and recovery effect reduction due to the gas mixing (Oldenburg 2003). Optimization studies were conducted on the operation strategy to obtain better gas recovery, e.g., locating the site for CO_2 injection at a depth below the level of natural gas production (Al-Hashami et al. 2005; Schütze et al. 2012).

The most well-known CO_2-EGR project is K12-B project in the Netherlands, where the gas mixture produced is separated and re-injected into the same gas reservoir at a depth of 3,800 m (van der Meer et al. 2005).

Increasing reservoir pressure in response to CO_2 injection induces mechanical stresses and deformations in the reservoir and cap rocks, which cause in return the changes of hydraulic properties and further the multiphase flow and storage behavior of the reservoir. Although temperature decrease and the corresponding cooling effects are limited in the near field of injection wells, fault slip may occur when the reservoir pressure rises to a critical level. This could lead to CO_2 leakage to drinking water source or even land surface and bring out significant environmental issues. Due to such reasons all the relevant aspects pertaining to geomechanical- and geohydraulic-coupled processes should be fully taken into consideration and numerically simulated prior to any CO_2 injection operations.

Although H^2M (two-phase flow and mechanical) coupled reservoir simulations were carried out in the early phases of CO_2 research, corresponding research related to injection and storage of CO_2 have been conducted mostly in recent years. To account for coupled THM processes in fractured and porous rocks under multiphase condition, Rutqvist and Tsang (2002) and Rutqvist et al. (2002) linked TOUGH2 with FLAC3D to investigate the stress changes and potential fault slip by CO_2-injection in saline aquifers. Khan et al. (2010) integrated VISAGE and ECLIPSE to investigate the caprock integrity of a potential carbon storage site and Ouellet et al. (2011) use this coupled code to simulate the CO_2 injection in saline aquifer at Ketzin, Germany. Li and Li (2010) linked FLAC to CMG's GEM to study the CO_2 enhanced coal bed methane (ECBM) recovery. Enhanced coal bed methane recovery was also studied in Connell and Detournay (2008) with coupling between coal bed methane simulator SIMED II and FLAC3D. However, the THM-coupled responses of reservoir and caprock formations to CO_2-injection into gas reservoirs have been minimally explored (Rutqvist et al. 2008; Taron et al. 2009).

The objective of this paper was therefore to study the THM-coupled responses of the storage formation and caprock, resulting from the reservoir pressure changes in the gas production, CO_2-EGR and CO_2-storage phase. The study focuses on the analysis of stress changes and deformations of the storage formation including the caprock integrity with due consideration to three different primary stress regimes: (1) the extensional ($\sigma_{H/h} = 0.8\sigma_v$), (2) the isotropic ($\sigma_{H/h} = \sigma_v$), and (3) the compressional stress state ($\sigma_{H/h} = 1.5\sigma_v$).

Thermodynamic and H^2M-coupled model

The THM-coupled simulation is performed with two different numerical simulators, the integrated code TOUGH2/EOS7C-FLAC3D, which is based on the TOUGH-FLAC simulator (Rutqvist et al. 2002), and OpenGeoSys (OGS) (Wang et al. 2011; Watanabe et al. 2012; Kolditz et al. 2012a, b).

In TOUGH-FLAC, the gas mixing process is simulated using the TOUGH2 EOS-module EOS7C (Fig. 1). EOS7C is an EOS-module which considers five mass components, namely water, brine, CO_2, tracer, and NCG (non-condensable gas, in this case CH_4). Cubic equations of state according to Peng–Robinson are adopted to calculate the density, enthalpy, and viscosity of the real gas mixture of the system H_2O–CO_2–CH_4. The partition of CO_2 and CH_4 between aqueous and gas phases is calculated using a very accurate chemical equilibrium approach. Darcy's law for multiphase flow is used to model the flow and transport of gas and aqueous phase mixtures taking into consideration of the Fick's diffusion law (Oldenburg et al. 2004).

The coupling concept in Rutqvist et al. (2002) is adopted to consider the geomechanical effects of the CO_2-EGR and CO_2-storage processes (Fig. 2). In every time step, TOUGH2 variables, including pressure and saturation are transferred to FLAC3D to calculate the deformation and stress redistribution in the rock formations. The new stresses and deformations of each element are then transferred back to TOUGH2 to calculate the corresponding changes of hydraulic properties. The concrete mathematical description of the used coupling concept is found in Rutqvist et al. (2002).

Governing equations in OGS

The general equation for balance of fluid or transported species mass is

$$\frac{\partial(\phi X_\alpha \rho)}{\partial t} + \nabla(\phi X_\alpha \rho u) + \nabla(i_\alpha) = Q \qquad (1)$$

for the porosity ϕ, bulk fluid density ρ, fluid velocity vector u, the solid mass fraction of the desired species X_α, a mass source term Q, and the diffusive/dispersive flux i_α. Utilizing Darcy's law, and taking into account that in

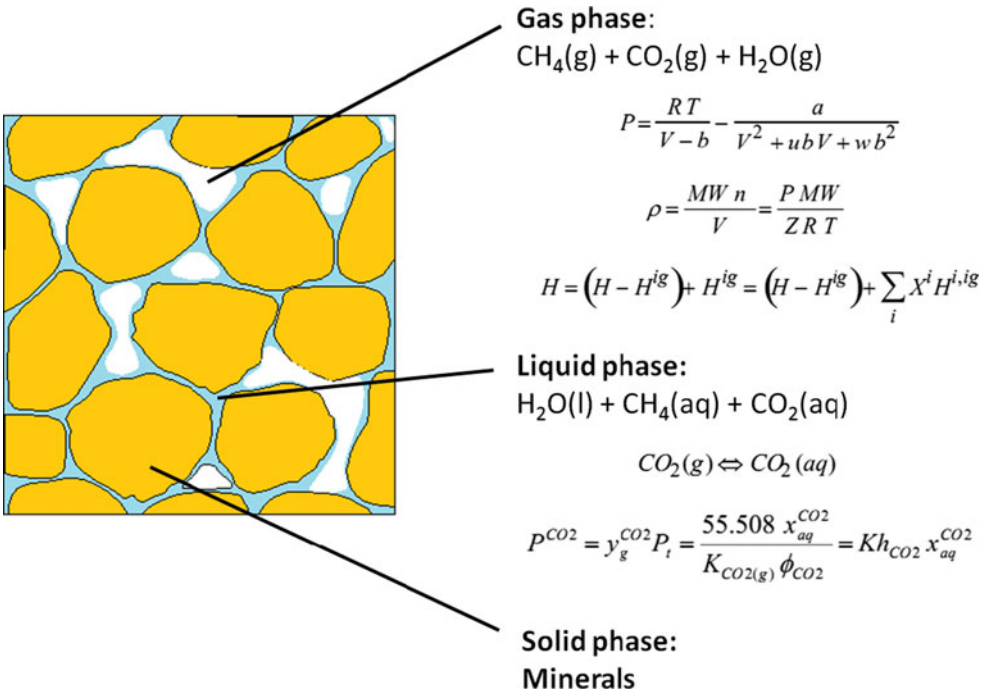

Fig. 1 EOS-module EOS7C in TOUGH2

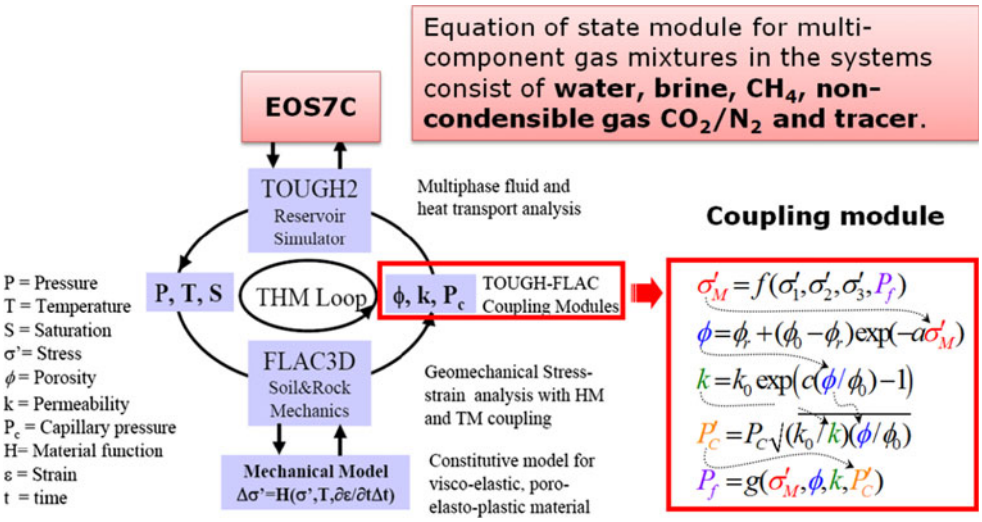

Fig. 2 Coupling concept from Rutqvist et al. (2002) combined with EOS7C

deformation problems the fluid velocity must be considered relative to the solid, we write

$$u_r = \phi(u - u_s) = -\frac{k}{\mu}(\nabla P - \rho g) \tag{2}$$

for the intrinsic permeability tensor k, the dynamic viscosity μ, and for velocity relative to the solid u_r, and the solid velocity u_s.

Balance of fluid mass

Substituting into Eq. 1 for $X = 1$ and negating the dispersive term, as we are considering total fluid balance (not transported species), yields,

$$\frac{\partial(\phi\rho)}{\partial t} + \nabla(\phi\rho u) = Q_f. \tag{3}$$

Substituting relative velocity into Eq. 3 and expanding the time derivative term and the resulting advection terms produces,

$$\phi\frac{\partial\rho}{\partial t} + \rho\frac{d_s\phi}{dt} + \nabla(\rho u_r) + \phi\rho\nabla(u_s) = Q_f \tag{4}$$

where, we have utilized the substantial derivative with respect to solid velocity, $d_s(A)/dt = \partial(A)/\partial t + u_s\nabla(A)$, for the variable A and have negated the term, $\phi u_s \nabla\rho$, based on an assumption of small strain ($u_s\nabla\rho \ll \partial\rho/\partial t$). Fluid density is dependent on both temperature and mass fraction of mixing gasses. We consider a binary gaseous system of

CO_2 and CH_4, where X represents the mass fraction of the invading species (CO_2) and $1 - X$ the fraction of in situ gas (CH_4). As the reservoir is maintained at constant temperature, its time and spatial derivatives may be rewritten as $\partial\rho/\partial(t,x) = \rho C_p \partial P/\partial(t,x) + \rho C_x \partial X/\partial(t,x)$, for respective fluid compressibilities, $\rho C_p = \partial\rho/\partial P$ and $\rho C_x = \partial\rho/\partial X$, where X is mass fraction of the invading gas species. Density and compressibility are calculated based on the ideal gas relationship, $\rho = (PM_{AB})/(z_{AB}RT)$ where M_{AB} is molecular weight of the mixture and z_{AB} is the mixture compressibility factor calculated from the Peng–Robinson equation of state, where parameters of the root equation are calculated from a standard binary mixing rule (i.e., Poling et al. 2001; Böttcher et al. 2012a, b). Additionally required is the balance of solid mass,

$$\frac{d_s\phi}{dt} = \frac{(1-\phi)}{\rho_s}\frac{\partial\rho_s}{\partial t} + (1-\phi)\nabla(u_s). \tag{5}$$

We utilize a Biot formulation to represent the solid density time derivative (in Eq. 5) as in (Rutqvist et al. 2001; Khalili and Selvadurai 2003) and substitute Eq. 5 and the density compressibility derivatives into Eq. 4 to obtain the final form of fluid mass balance,

$$\left(\phi\rho C_p + \rho\frac{\alpha-\phi}{K_g}\right)\frac{\partial P}{\partial t} + (\phi\rho C_x)\frac{\partial X}{\partial t} + \nabla(\rho u_r) = Q_f - \alpha\nabla(u_s) \tag{6}$$

to be solved for two primary variables, P and X, with $\nabla(u_r)$ given by Eq. 2, where the solid strain rate ($\nabla(u_s) = \dot{\varepsilon}$) is given by balance of solid momentum in the mechanical deformation equation, and for the solid grain modulus, K_g, and the Biot coefficient $\alpha = 1.0 - K/K_g$, for the solid material drained bulk modulus K.

Balance of chemical mass

Diffusive/dispersive flux of gaseous species with respect to mass fraction is assumed to follow Fick's first law (Bauer et al. 2006; Ho and Webb 2006), $\nabla(i) = -\phi\rho D\nabla X$, relative to a fixed coordinate system and recoverable from the Stefan–Maxwell equations for a binary system. Diffusivity of gasses is calculated based on temperature and pressure from kinetic gas theory (Atkins and de Paula 2002) for a CO_2 and CH_4 binary system. Based on the formulation attributed to Chapman and Enskog, the method for calculating the binary diffusion coefficient can be found in (Poling et al. 2001). The effective diffusivity D^*, is corrected for tortuosity (in a fully gaseous system) based on Millington and Quirk (1961), relative to the binary diffusion coefficient $D^* = \phi^{1/3}D_{AB}$. Total dispersion D, may potentially also include contribution from longitudinal and transverse dispersion coefficients or may simply adopt the diffusive value, $D = D^*I$.

Expanding Eq. 3 with respect to ϕ, ρ, and u, and rearranging for $\partial\rho/\partial t$, and then substituting this into the expanded form of Eq. 1 results in,

$$\phi\rho\frac{\partial X}{\partial t} + \phi\rho u\nabla(X) + \nabla(i_\alpha) + XQ_f = Q_x \tag{7}$$

Substituting for diffusive flux and for relative fluid velocity yields the final form of balance of species mass,

$$\phi\rho\frac{\partial X}{\partial t} + \rho u_r\nabla(X) - \nabla(\phi\rho D\nabla X) + XQ_f = Q_x \tag{8}$$

where we have assumed, as before, that the term $u_s\nabla X \ll \partial X/\partial t$, by the requisite of small strain.

Balance of solid momentum

The solid displacement equations are more understandably written in summation convention, which we adopt for this section only. Beginning with the concept of effective stress, $\sigma'_{ij} = \sigma_{ij} + \alpha P\delta_{ij}$, for the effective stress σ', and total stress σ, negative in compression, we then write the balance of solid momentum, $\partial\sigma_{ij}/\partial x_i + F_i = 0$, with the body force F. From the definition of strain, $\varepsilon_{ij} = (\partial u_i/\partial x_j + \partial u_j/\partial x_i)/2$, the displacement formulation of mechanical equilibrium may be written for a linear elastic solid,

$$\frac{\partial}{\partial x_i}\left[G\frac{\partial u_i}{\partial x_j} + (\lambda+G)\frac{\partial u_j}{\partial x_i} - \alpha P\delta_{ij}\right] = -F_i \tag{9}$$

for the shear modulus G, and Lamè constant λ.

Solution procedure

Because of the high non-linearity of the density-dependent flow equations, we have found the best solution to be a monolithic coupling between the balances of fluid and transported mass equations, with a staggered coupling to the equation of mechanical equilibrium. Time step is controlled independently for the two systems based upon the rate of change of respective primary variables, with the mechanical equilibrium calculation occurring infrequently relative to the very strongly coupled density equations. In fact, in very long-term problems the direct impact of solid displacement on the fluid equations via the strain rate term is not significant, and the strongest influence from the mechanical system occurs via changes to porosity and permeability.

The global mass balance equation takes shape as

$$\begin{bmatrix} C_{pp} & C_{px} \\ C_{xp} & C_{xx} \end{bmatrix}\begin{Bmatrix} \dot{P} \\ \dot{X} \end{Bmatrix} + \begin{bmatrix} M_{pp} & M_{px} \\ M_{xp} & M_{xx} \end{bmatrix}\begin{Bmatrix} \nabla P \\ \nabla X \end{Bmatrix} + \nabla\cdot\begin{bmatrix} K_{pp} & K_{px} \\ K_{xp} & K_{xx} \end{bmatrix}\begin{Bmatrix} \nabla P \\ \nabla X \end{Bmatrix} = \begin{Bmatrix} Q_f - \alpha\dot{\varepsilon} \\ Q_x \end{Bmatrix} \tag{10}$$

discretized in space with standard Galerkin finite elements, and in time with a generalized first-order finite-difference scheme. Coupling to the mechanical system occurs on the right-hand-side of the fluid system, via the solid strain rate, and within the mechanical system via the effective stress. Non-linearities are handled with a Picard or Newton linearization, although Picard is sufficient for the problem presented here, provided the flow-transport system is treated monolithically.

In OGS, simulations are conducted in a dry reservoir at a constant temperature of 53 °C, with gas thermodynamics corresponding to those in EOS7C. The gas flow equation is coupled monolithically to a fractional mass transport equation, with fluid properties governed by a binary mixing rule for the CO_2–CH_4 system and calculated with the Peng–Robinson equation of state (Böttcher et al. 2012a, b).

Hydro-mechanical parameters

Both simulators are fit with the same constitutive laws regarding porosity and permeability change for these simulations. Hydraulic properties are correlated with the effective mean stress using Eqs. 11 and 12 and parameters from Rutqvist and Tsang (2002):

$$\phi = \phi_r + (\phi_0 - \phi_r)\exp\left(-a\sigma'_m\right) \tag{11}$$

$$k = k_0 \exp\left[c\left(\frac{\phi}{\phi_0} - 1\right)\right] \tag{12}$$

where

ϕ_0	Zero stress porosity
ϕ_r, ϕ	Residual and actual porosity
k_0, k	Zero-stress permeability and actual permeability (m^2)
$\sigma'_m = (\sigma_m - \alpha p)$	Effective mean stress (MPa)
σ_m, p	Mean stress and pore pressure (MPa)
a, c	Material constants ($a = 5 \times 10^{-2}$ MPa^{-1}, $c = 22.2$)

In order to consider the influence of plastic dilatancy ε^p_{vol} on the permeability, an extra term is multiplied by the original function (Gou 2011)

$$k = k_0 \times \exp\left[c\left(\frac{\phi}{\phi_0} - 1\right)\right] \times \exp\left[b \cdot \varepsilon^p_{vol}\right] \tag{13}$$

Here b is a constant and assumed to be 2,300, which causes a permeability increase by ten times with a plastic volumetric strain of 0.1 %. These newly updated hydraulic properties are then used in the TH-coupled simulation in TOUGH2 for the next time step and directly in the flow equation of OGS for the next non-linear iteration.

Simulation model and process

A generic 3D simulation model (20,000 × 3,000 × 100 m) was generated. For TOUGH-FLAC, this was discretized into 3,344 structured cells (Fig. 3). For the OGS finite element solution, an unstructured mesh was generated that attempted to utilize nearly the same number of cells as the finite difference solution, while maintaining reasonable element aspect ratios and sufficient element quality. The result is a mesh with 8,078 elements in precisely the same geometric layout as the

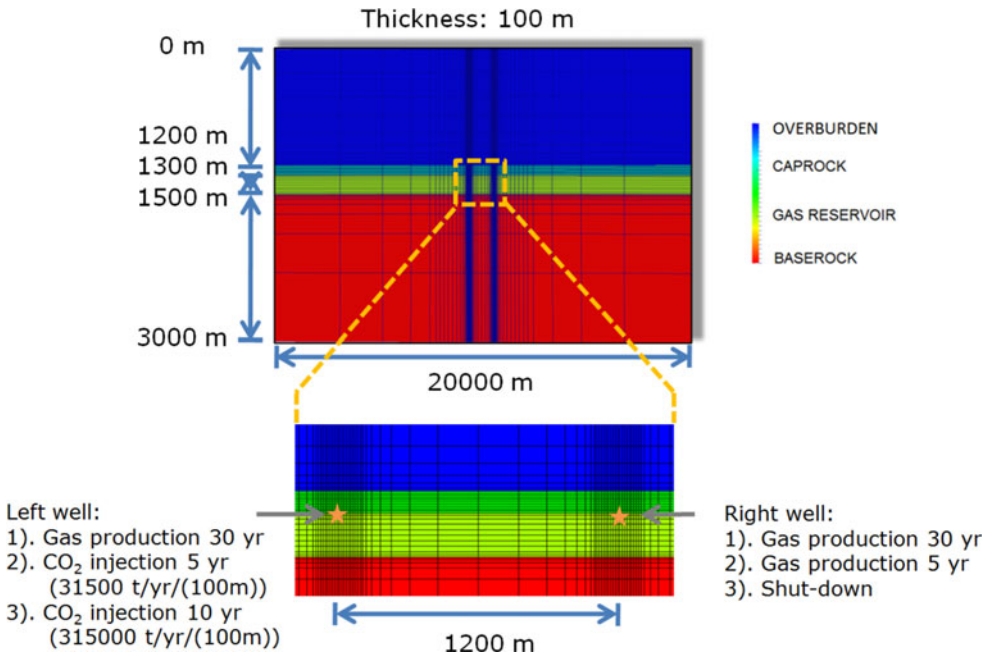

Fig. 3 Generic 3D planar model for TOUGH-FLAC simulation (vertically exaggerated)

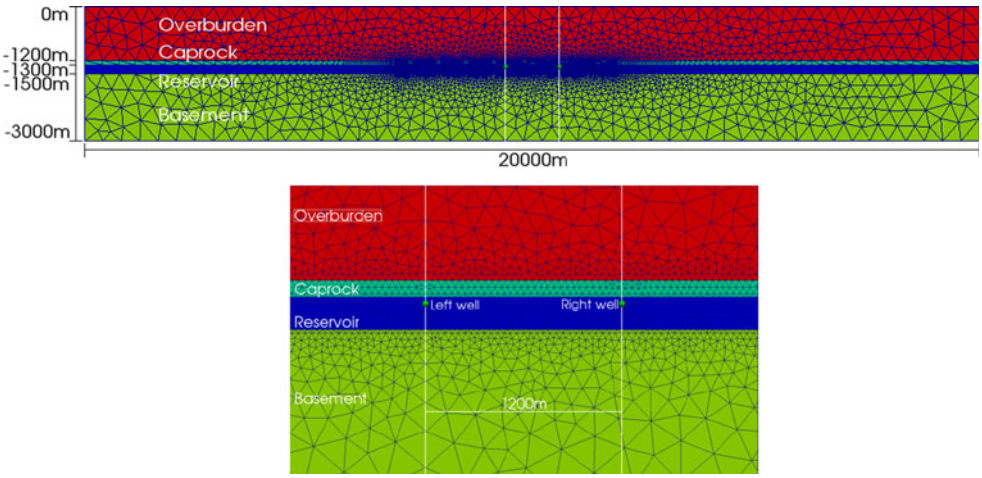

Fig. 4 Generic 3D planar model in the OGS simulations

TOUGH-FLAC solution (Fig. 4). The whole model includes four horizontal rock layers from top to bottom, namely overburden (1,200 m Buntsandstein), caprock (100 m claystone), gas reservoir (200 m sandstone), and base rock (1,500 m vulcanite). Two wellbores for production and injection are 1,200 m apart in the horizontal direction and are drilled to a depth of 1,300 m, the upper surface of the reservoir layer.

All rock layers are assumed as elasto-plastic materials in the TOUGH-FLAC simulations (using Mohr–Coulomb model) and as elastic materials in the OGS simulations. The parameters are listed in Table 1. The initial porosity and permeability under the effective primary stresses are calculated after Eqs. 1 and 2 using the effective primary mean stress, the zero stress porosity, and permeability. Since the effective primary mean stress in each rock layer is not constant and is a function of depth, the porosity and permeability of the reservoir formation vary in the range of 0.0928–0.0935 and 1.2–1.4 D, respectively.

The whole simulation consisted of 30-year production, 5-year CO_2-EGR, and 1-year CO_2-storage. In TOUGH-FLAC, the model was first initialized with a hydrostatic pore pressure distribution while the reservoir, consisting only of single phase gas, was given an initial pore pressure of 13 MPa and temperature of 53 °C. In OGS, where simulations do not consider the presence of a water phase, the hydrostatic gradient was allowed to evolve naturally, by running the first several time steps without fluid or solid storage, from an initial uniform pressure of 13 MPa, which allows a nearly instantaneous development of pressure distribution. The overburden was considered to be fully water saturated and the remainder of the domain fully gas saturated. This allows pressure to evolve to the same hydrostatic value at the top of the caprock layer as for TOUGH-FLAC.

Then gas production of CH_4 was performed from both wells with a fixed bottomhole pressure of 5 MPa for 30 years. After the 30-year production, CO_2 was injected into the left well at a rate of 31,500 tons/year, while the well on the right was constantly kept in production of the gas at the same bottomhole pressure (this occurs from year

Table 1 Mechanical and hydraulic properties of the rock formations in the calculation model

Properties	Overburden	Caprock	Reservoir	Base rock
Rock density ρ (kg/m^3)	2,260	2,720	2,460	2,700
Young's modulus E (GPa)	10.0	22.1	21.2	85.0
Poisson's ratio ν (–)	0.25	0.214	0.129	0.26
Friction angle φ (°)[a]	30.0	22.0	29.0	– (Elastic)
Cohesion c (MPa)[a]	20	26	11.9	– (Elastic)
Biot's coefficient α (–)	1	0.358	0.645	1
Zero-stress porosity ϕ_0 (–)	0.1	0.01	0.1	0.01
Residual porosity ϕ_r (–)	0.09	0.009	0.09	0.009
Zero-stress permeability k_0 (m^2)	3×10^{-15}	6×10^{-20}	6×10^{-12}	7×10^{-20}
Corey's S_{gr} (–)[a]	0.05	0.05	0.05	0.05
Corey's S_{lr} (–)[a]	0.3	0.3	0.3	0.3
Van Genuchten's p_0 (kPa)[a]	6.211	621.1	19.88	621.1
Van Genuchten's λ (–)[a]	0.457	0.457	0.457	0.457

[a] Parameters used only in the TOUGH-FLAC simulations

30 to 35). A CO_2-storage phase was then initiated at the 35-year mark in which the right well was sealed and CO_2 further injected into the left well at a rate of 315,000 tons/year (occurring from year 35 to 40).

Simulator differences

There are several fundamental differences between the TOUGH-FLAC and OGS simulators, some of which will have a small impact on the results presented below. First, OGS is a fully finite element (FEM) simulator, while TOUGH2 is an integral finite difference scheme. This will lead to slight differences in the numerical dispersion of the simulators. TOUGH2 is fully upwinded with respect to mass transport, while for these simulations OGS utilizes a standard Galerkin FEM procedure (Park et al. 2011), with dispersion introduced via coefficients of dispersion designed to maintain the Peclet number near 2.0, and thus produce dispersive characteristics similar to an upwinded scheme. Both codes include molecular diffusion of gasses (utilizing a binary gas molecular diffusion calculation). Coupling between the fluid and solid equations occurs at the gauss point level within the Gaussian integration scheme of OGS, while in TOUGH-FLAC, element center properties of TOUGH2 are interpolated to nodal values for the stress calculation in FLAC.

Second, OGS here utilizes single-phase fractional mass transport of gaseous species (see the above equation system) in a monolithic coupling with the fluid transport equation and TOUGH2 uses two-phase fractional transport in a staggered Newton–Raphson scheme with the flow equation. To maintain a similar pressure evolution, the overburden fluid is assumed to be water (as for TOUGH-FLAC). Because some CO_2 is expected to penetrate the base rock, it is not possible to assume water saturation here, and instead all areas below the overburden are initially gas saturated. This will lead to some differences in the way that pressure from the base rock serves as replenishment to the under pressured reservoir.

Simulation results and discussion

After 30-year gas production, the reservoir pressure was reduced from 13 to 5 MPa in both simulators. The total produced gas was roughly 2,260,000 tons (3,183 MMSCM) in the production element of TOUGH-FLAC and lower value of 1,440,000 tons at the production node of OGS. This discrepancy may be due to the presence of a water phase in the base rock of the TOUGH-FLAC solution, which would serve as a replenishment of pressure that behaves differently in the OGS solution, but this will require further investigation. These values are comparable with the analytically estimated gas production according to the thermodynamic condition and stress state. The total gas recovery rate after 30-year production was estimated at 63.5 %.

Figure 5 shows the time-dependent gas production rate and CO_2 mass fraction in the produced gas during the CO_2 injection phase for the TOUGH-FLAC solution and Fig. 6 for the OGS solution. Stationary production was reached after 1 year and the first CO_2 breakthrough occurred 1.5 years after the start of CO_2-injection in both simulators. After 5 years of injection, CO_2 mass fraction in the produced gas rose to 8 % and CO_2-EGR was stopped. The OGS solution ceased EGR at the same time despite having much larger CO_2 mass fractions in the produced fluid. The injected CO_2 was 158,000 tons (81 MMSCM) identically in both simulators (both utilized the same injection rate) while total produced gas during the 5-year CO_2-EGR was 49,200 tons (69 MMSCM) in TOUGH-FLAC and nearly

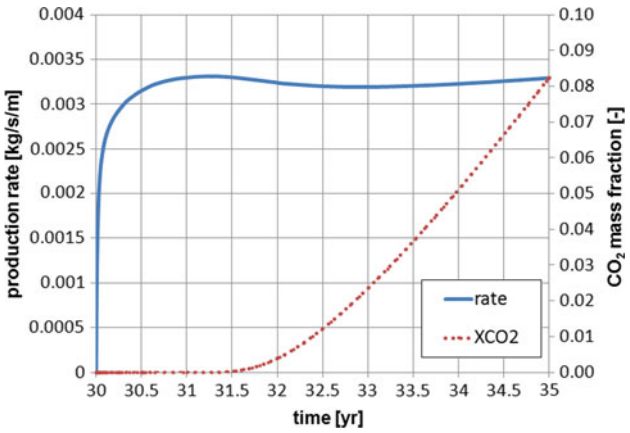

Fig. 5 TOUGH-FLAC: CO_2 mass fraction (*X*CO2) in the gas mixture during the whole CO_2-EGR process

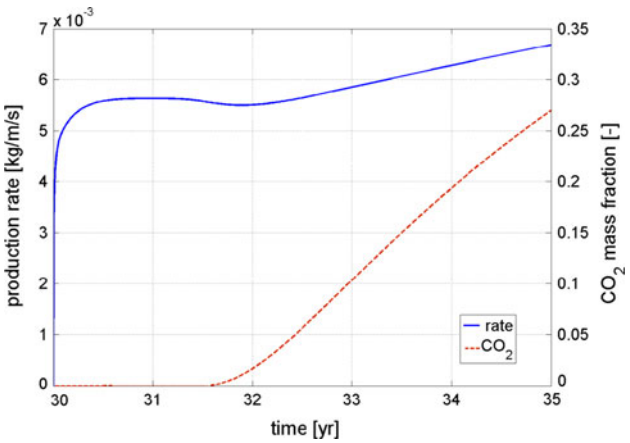

Fig. 6 OpenGeoSys: CO_2 mass fraction (*X*CO2) in the gas mixture during the whole CO_2-EGR process

double this value (102,000 tons) in OGS (see also Figs. 5, 6). This value is much larger than 158 tons (0.2 MMSCM), which was simulated with neither changes of bottom hole pressure nor CO_2-injection. For TOUGH-FLAC the volume ratio CO_2/CH_4 (SCM/SCM) was about 1.16 and the gas recovery rate increased by 1.4 %. But these results were based on the fact that the injector and producer are 1,200 m apart. A larger distance between them will delay the CO_2 breakthrough, which makes the EGR effect better. With a well distance of 5 km the recovery rate increase is estimated at 5.83 %.

Figure 6 shows time-dependent production for the OGS solution. Like TOUGH-FLAC, steady production occurs after approximately 1 year at a similar magnitude, but higher value of 0.0056 kg/s/m. Carbon dioxide breakthrough occurs at nearly the same time of 1.5 years, but the arrival front is much steeper and obtains a higher fraction of CO_2 in the produced fluid.

Figure 7a–d show the CO_2 mass fraction in the gas mixture within the 5-year CO_2-EGR (Fig. 7a–c) and at the end of CO_2-storage (Fig. 7d) for TOUGH-FLAC. Figure 8 is an identical display for OGS. It is clearly seen how CO_2 moves down from the injection point due to its large density in comparison with CH_4 at the same thermodynamic conditions.

In the TOUGH-FLAC solution during the whole CO_2-EGR process the reservoir pressure remained unchanged (5 MPa). Under this reservoir pressure, there is still no obvious CO_2–CH_4 interface in the gas mixture. At the end of 5-year CO_2-EGR the maximal CO_2 mass fraction in the gas mixture reaches roughly 80 % (only near the injection well). With further CO_2-injection during CO_2-storage the reservoir pressure increased from 5 to 8 MPa. Most of the reservoir is occupied by CO_2 (CO_2 maximal fraction reached 99 %). Most of CH_4 is located directly under the caprock due to buoyancy effect and CO_2 at the bottom.

For the OGS solution, behavior is quite similar during the EGR and storage phases. During EGR, the reservoir pressure remains essentially unchanged at 5 MPa and CO_2 mass fractions of roughly 80 % are achieved near injection. During CO_2 storage the reservoir pressure increases from 5 to 7.9 MPa, or nearly the same as for TOUGH-FLAC. Much of the reservoir is completely saturated with CO_2 at the end of the storage phase.

We now proceed to examine in more detail the mechanical consequences of injection. Figure 9 (TOUGH_FLAC) and Fig. 10 (OGS) show stress changes along the vertical line from the injection point at end of the CO_2-storage process, resulting from the reservoir pressure increase from 5 to 8 MPa. The total vertical stress slightly increased (<0.1 MPa), while the effective vertical stress decreased by 2 MPa due to the reservoir pressure increase of 3 MPa. However, the horizontal stress had the opposite tendency. The horizontal effective stress slightly changed due to a Biot's coefficient ($\alpha = 0.645$), while the total stress increased by 1.7 MPa. There are only small differences here between the two simulators. In the TOUGH-FLAC simulation a Mohr–Coulomb model was adopted for elasto-plasticity, but during the whole process no plastic deformation was observed, i.e., the reservoir and caprock

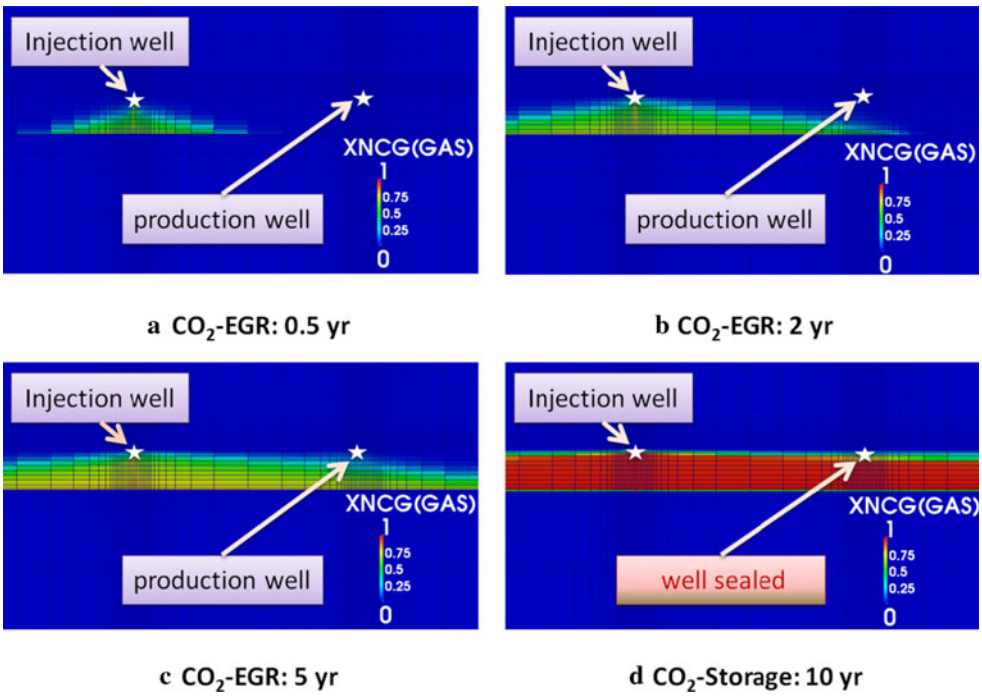

Fig. 7 TOUGH-FLAC: CO_2 mass fraction in the gas mixture at different times of the CO_2-EGR process

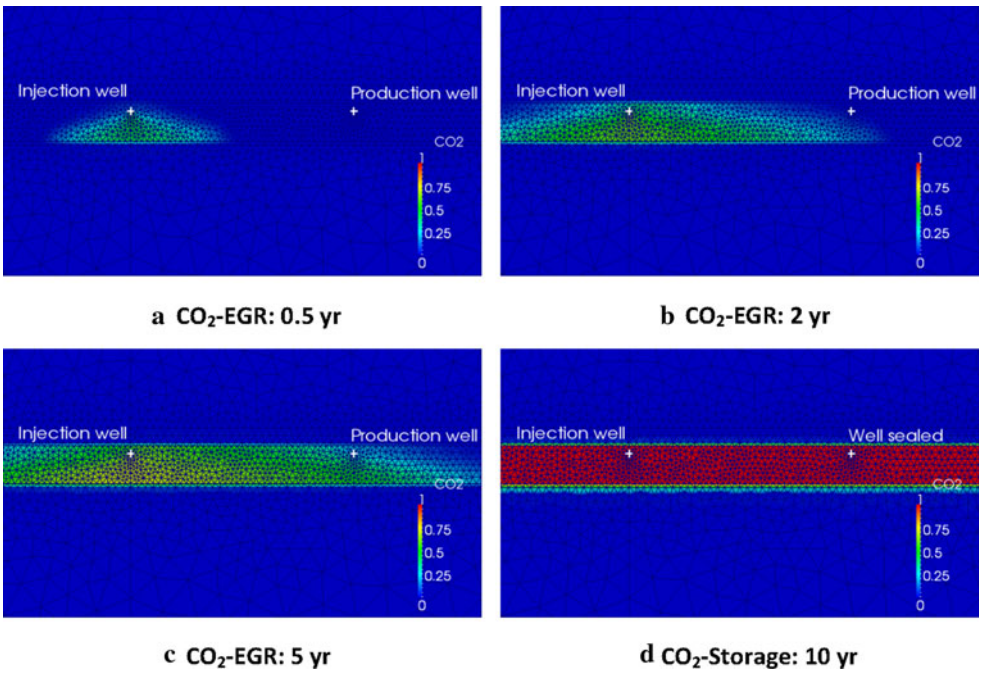

Fig. 8 OpenGeoSys: CO_2 mass fraction in the gas mixture at different times of the CO_2-EGR process

behaved elastically. The OGS solution was conducted under fully elastic conditions. There is an analytical solution for the stress change under this condition according to Hou et al. (2009):

$$\Delta\sigma_{\mathrm{H/h}} = \alpha\frac{1-2v}{1-v}\Delta p \tag{14}$$

$$\Delta\sigma_{\mathrm{z}} = 0 \tag{15}$$

where

$\Delta\sigma_{\mathrm{H/h}}$ Change of total horizontal stresses in MPa
α Biot's coefficient (values see Table 1)
v Poisson's ratio (values see Table 1)
Δp Pore pressure change in MPa
$\Delta\sigma_{\mathrm{z}}$ Change of total vertical stresses in MPa

The calculated horizontal stress change in the reservoir (ca. 1.65 MPa after Eq. 14) agrees well with the numerically simulated result (ca. 1.7 MPa). The maximal change ($\sim$0.3 MPa) of the horizontal stresses in caprock is very small in comparison with that in the reservoir. That means the caprock integrity is not influenced at all. Furthermore, neither pore pressure nor stress in overburden changes during the 15-year CO_2-injection.

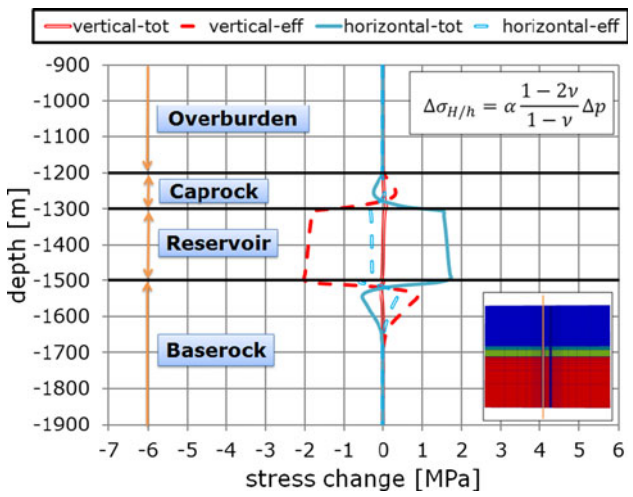

Fig. 9 Stress change along the vertical line through the injection point during the CO_2-storage phase for TOUGH-FLAC (positive change indicates an increase in compressive stress)

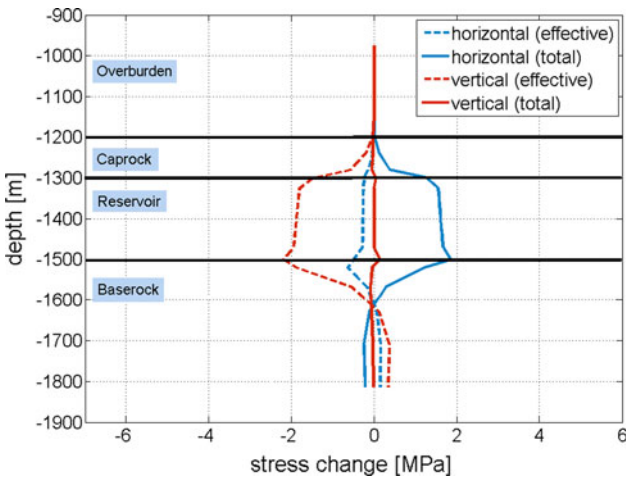

Fig. 10 Stress changes along a vertical line through the injection point during the CO_2-storage phase for OGS (positive change indicates an increase in compressive stress)

Figure 11 shows the stress paths at the injection point for three different primary stress regimes.

After 45 years, none of the stress paths had reached the strength of the reservoir rock, which has an internal friction angle of 29° and cohesion of 11.9 MPa. It is clearly seen that the stress states for the whole process, namely 30 years' production, 5 years' CO_2-EGR and 10 years' CO_2-storage, in all three different primary stress regimes are far away from the reservoir rock strength, although the used strength of the reservoir rock is much lower than the strength of the Northern German sandstone, e.g., in Hou et al. (2009). Since the reservoir formation is still in the range of elastic condition, the further stress path till the plastic state could be quantitatively predicted according to Eqs. 14 and 15. The predicted stress paths are presented in Fig. 11. The maximal and minimal effective stress at the end of production phase ($t = 30$ year) for both extensional and isotropic primary stress regimes are in the vertical and horizontal direction, respectively, and the in situ effective stress factor $\left[\Delta\sigma'_{\min}/\Delta\sigma'_{\max} = v/(1-v)\right]$ is smaller than one $\left(\sigma'_{\max} = \sigma'_z, \sigma'_{\min} = \sigma'_h\right)$. So $\sigma'_{\max}$ decreases faster than $\sigma'_{\max}$, which cause the stress paths move directly toward the isotropic effective stress line with further pressure rise (but never exceed it because $\sigma'_{\max} \geq \sigma'_{\min}$). When it reaches this isotropic line, the directions of the maximal and minimal effective stress will switch $\sigma'_{\max} = \sigma'_{H/h}, \sigma'_{\min} = \sigma'_z$. The corresponding pore pressure increases are listed in Table 2. After that both extensional and isotropic primary stress regimes switch to the compressional regime and the corresponding stress paths will move away from that isotropic line and toward the σ'_1 axes. With further injection the stress paths would cross the σ'_1 axes at first but not the rock strength line. According to this analysis tension failure in the reservoir would occur (if we assume the rock tension strength is zero), but shear failure will never happen even with further CO_2-injection.

As scenario study a worse case is analyzed, namely the reservoir is assumed as naturally fractured (although such sandstone formation does not really exist in Germany). As a conservative assumption, the strength of such fractured reservoir formations has just a small internal friction angle of 20° and zero cohesion (Fig. 10). It reveals that potential fracture slip in such reservoirs could occur for all of the three primary stress regimes. The sequence of three stress paths reaching the strength of the fractured reservoir formation is compressional, isotropic, extensional, and the corresponding pore pressure rises are 13.26, 28.34, and 33.18 MPa (Table 3). But the maximal storage pressure is also restricted by the barrier integrity criteria. Here the allowed storage pressure is calculated with simultaneous consideration of both tensile fracture and penetration criteria according to Hou et al. (2009), namely

$$\max\ p_s = \min \left\{ \begin{matrix} p_h + p_e \\ \sigma_h \end{matrix} \right\} \Big/ n \tag{16}$$

Table 2 Predicted pore pressure increase for the stress regime conversion (isotropic to compressional)

	Compressional	Isotropic	Extensional
Reservoir pressure p (MPa)	–	14.88	25.61
Reservoir pressure increase Δp (MPa) from begin of CO_2-storage	–	9.88	20.61

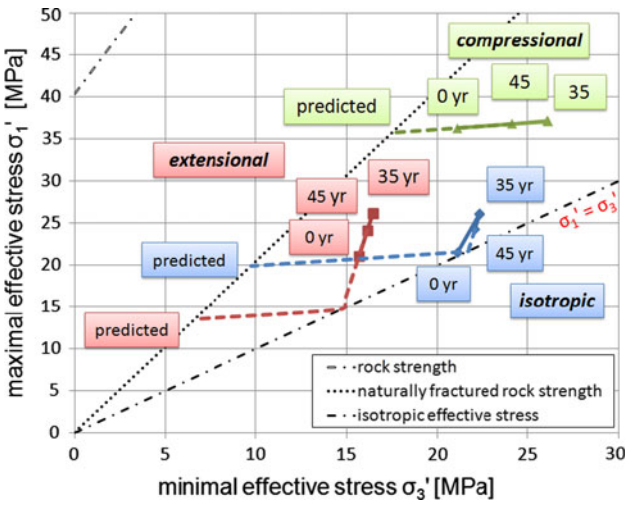

Fig. 11 Stress paths of the injection point for three different primary stress states

Table 3 Predicted maximal storage pressure

	Compressional	Isotropic	Extensional
Reservoir pressure p/pressure increase Δp (MPa) from begin of CO_2-storage (scenario case: shear failure in a naturally fractured reservoir)	18.26/13.26	33.34/ 28.34	38.18/ 33.18
Maximum reservoir pressure after penetration criterion ($p_h + p_e$)	17	17	17
Primary horizontal stress at the Caprock bottom (MPa)	43	28	22
Predicted maximum storage pressure ($n = 1.25$) (MPa)	13.6	13.6	13.6

where

p_s Storage pressure
p_h Hydrostatic pressure at caprock bottom in MPa (here 13 MPa)
p_e Entrance (dry to wet fluid) pressure in MPa (here 4 MPa)
σ_h Primary minimal horizontal stress at caprock bottom
n Safety factor (1.25)

As shown in Table 3 the possible reservoir pressure based on the penetration criterion is 17 MPa for all three primary stress regimes. The minimal horizontal stresses in caprock bottom are 43, 28, and 22 MPa, respectively. So the maximal allowed storage pressure for CO_2-storage is determined by the penetration criterion with consideration of a safety factor, e.g., 1.25, namely 13.6 MPa. With Consideration of the 3 MPa pressure rise due to 3.15 million ton CO_2-injection, another 5.88 million ton CO_2 could be injected.

Figure 12 (TOUGH-FLAC) and Fig. 13 (OGS) show the vertical displacements of selected points under and above the injection point. P1 locates at the ground surface and P2, P3, and P4 at the interface between overburden, caprock, reservoir, and base rock. The ground surface and caprock top (P1 and P2) have similar displacement (5 cm downward in TOUGH-FLAC and 6.5 cm in OGS) resulting from the gas production and recover upward (nearly 2 cm recovery in both simulators) due to CO_2-injection. The reservoir top (P3) has the similar displacement tendency, while the reservoir bottom (P4) moves downward during the CO_2-EGR and CO_2-injection phases and reaches 0.2 cm at the end of 45 years in TOUGH-FLAC as water is depleted in the base rock towards the under pressured reservoir. In OGS, this value is much larger (1.3 cm),

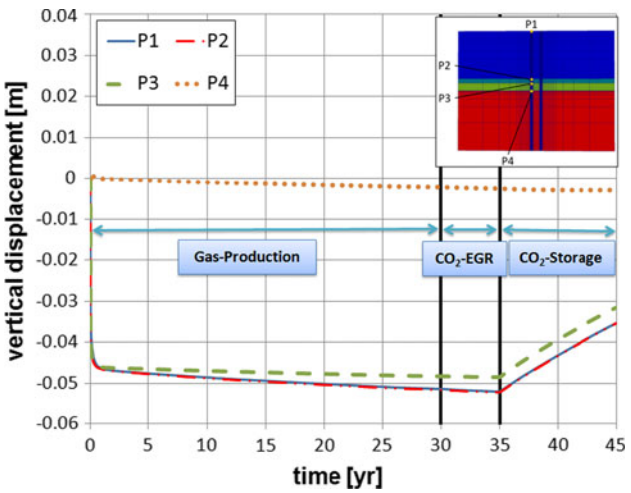

Fig. 12 Displacement of selected points above and under the injection point (TOUGH-FLAC)

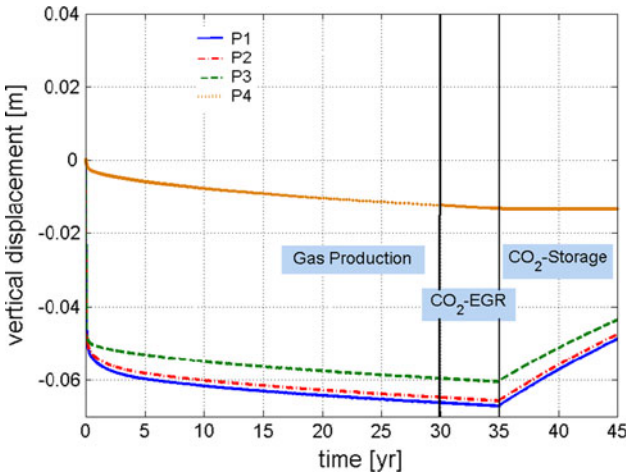

Fig. 13 Displacement of selected points above and under the injection point (OGS)

which is as expected for a gas saturated base rock that is more compressive than one that is water saturated, and requires a greater volume of gas depletion to recover reservoir pressure than is the case for water.

The compaction of the rock formation could be calculated from the displacement difference between P1–P2, P2–P3, and P3–P4, e.g., the reservoir has a compaction $\Delta\varepsilon_z$ (P3–P4) of 0.023 % in TOUGH-FLAC and 0.0236 % in OGS at the end of the production and after 10 years' CO_2-injection 0.0143 % in TOUGH-FLAC and 0.015 % in OGS. This value could be analytically calculated according to Hou et al. (2009):

$$\Delta\varepsilon_z = -\frac{\alpha\Delta p}{E}\frac{(1-2v)(1+v)}{1-v} \tag{17}$$

The calculated reservoir compactions after Eq. 17 are correspondingly about 0.023 and 0.0146 % which are comparable with the numerically simulated values.

Conclusions

Several conclusions have been drawn from the thermodynamic and H^2M-coupled simulations of a generic 3D planar model using the integrated code "TOUGH2/EOS7C-FLAC3D" and the multi-purpose TH^2M/C simulator OGS. Both simulators agree on these conclusions and furthermore show very similar results in all stages of the tests.

1. With the CO_2-injection of 0.158 million ton during CO_2-EGR the natural gas recovery rate increased by 1.4 %. A better EGR effect could be achieved by increasing the distance between injection and production wells (e.g., 5.83 % for a distance of 5 km instead of 1.2 km in this study).

2. The solution indicates that the CO_2-EGR operation will not cause changes in the reservoir pressure, mainly due to the balanced injection rate and the high compressibility of the gas, while CO_2-storage will cause an increase in the reservoir pressure from 5 to 8 MPa in response to 3.15 Million ton CO_2-injection without parallel production. Density differences between the fluids will result in a clear separation of CO_2 and CH_4 in the reservoir at the bottom and top, respectively.
3. In the CO_2-storage phase, the total vertical stress in the reservoir increases marginally, while the effective vertical stress change is relatively high (till 2 MPa). Conversely, the total horizontal stress increases about 1.7 MPa in response to the reservoir pressure rise of ca. 3 MPa, while the effective horizontal stress will show only little change. Both analytical and numerical results of stress changes are comparably similar. The maximum stress change in the caprock is less than 0.3 MPa, much smaller than that in the reservoir, while the overburden has still the primary stress state.
4. At all operation stages there are no evidence of plastic deformations under the considered conditions and both reservoir and caprock behave elastically. Based on the stress path analysis, the tension failure in the reservoir formation could occur but the shear failure of the intact rock will never happen with further CO_2-injection.
5. A special case is analyzed with the assumption that the reservoir is naturally fractured (conservatively assumed strength: internal friction angle of 20° and zero cohesion). The critical reservoir pressures for a shear failure of this naturally fractured reservoir are 18.26, 33.34, and 38.18 MPa for the compressional, isotropic, and extensional primary stress regime, respectively. However, the maximal allowed storage pressure 13.6 MPa is determined by the penetration criterion. This allows another 5.88 Million ton CO_2 to be injected.

However, the influences of faults and non-isothermal effects are not simulated numerically in this study. The corresponding research work is ongoing.

Differences between the two simulators arise with regard to CO_2 breakthrough (sharper breakthroughs in OGS) and production rate (slightly higher in OGS), and the rate of pressure recovery in the reservoir due to the influx of fluid from the base rock. The OGS result shows greater mechanical displacement at the base of the reservoir. These last two are explainable by the single-phase solution provided by OGS, where a gas-dominated base rock will behave differently than one that is water saturated.

These differences will require further investigation, and in fact introduce the possibility for further benchmarking. The problem presented in this paper serves as an excellent benchmark for further code comparisons of H^2M or TH^2M behavior during CO_2 injection.

Acknowledgments The work presented in this benchmarking paper is contributed from a number of projects, funded partially by the German Federal Ministry of Education and Research (BMBF), GEOTECHNOLOGIEN program (Grants 03G0704Q, 03G0704S), A-DUR project (Grant 02E10588), PROTECT/CO2BENCH (Grant 03G0797D) and the Sino-German Center for Research Promotion (Grant GZ573), which is funded jointly by the National Natural Science Foundation of China (NSFC) and the German Research Foundation (DFG).

References

Al-Hashami A, Ren SR, Tohidi B (2005) CO_2 injection for enhanced gas recovery and geo-storage: reservoir simulation and economics. In: Proceedings of the SPE Europec/EAGE annual conference, SPE 94129, Madrid, pp 13–16

Atkins P, de Paula J (2002) Atkins' physical chemistry, 7th edn. Oxford University Press, Oxford, p 1149

Bauer S, Beyer C, Kolditz O (2006) Assessing measurement uncertainty of first-order degradation rates in heterogeneous aquifers. Water Resour Res 42(1):W01420. doi:10.1029/2004WR003878

Böttcher N, Singh AK, Kolditz O, Liedl R (2012a) Non-isothermal compressible gas flow for the simulation of an enhanced gas recovery application. J Comput Appl Math. doi:10.1016/j.cam.2011.11.013

Böttcher N, Kolditz O, Liedl R (2012b) Evaluation of equations of state for CO_2 in numerical simulations. Environ Earth Sci, accepted (this issue)

Connell LD, Detournay C (2008) Coupled flow and geomechanical processes during enhanced coal seam methane recovery through CO_2 sequestration. Int J Coal Geol 77:222–233

Gou Y (2011) Untersuchungen zu THM-gekoppelten Reaktionen der Speicherformation und des Deckgebirges bei CO2-EGR mit dem integrierten Code TOUGH2–FLAC3D. Masterarbeit am Institut für Erdöl- und Erdgastechnik der TU Clausthal

Ho CK, Webb SH (eds) (2006) Gas transport in porous media. Springer, New York, p 446

Hou Z, Tadongmo FA, Pusch G (2009) Secondary in situ stresses resulting from change of pore pressure influence on the maximal storage pressure of CO_2 or natural gas in reservoirs. DGMK/ÖGEW-Frühjahrstagung band, Celle, pp 325–336

IEA (2004) Prospects for CO2 capture and storage

IPCC (2005) IPCC special report on carbon dioxide capture and storage

Khalili N, Selvadurai APS (2003) A fully coupled constitutive model for thermo-hydro-mechanical analysis in elastic media with double porosity. Geophys Res Lett 30(24):1–5

Khan S, Han H, Ansari SA, Khosravi N (2010) An integrated geomechanics workflow for Caprock-integrity analysis of a potential carbon storage. In: SPE international conference on CO_2 capture, storage, and utilization, SPE 139477-MS

Kolditz O, Bauer S, Bilke L, Böttcher N, Delfs JO, Fischer T, Görke UJ, Kalbacher T, Kosakowski G, McDermott CI, Park CH, Radu

F, Rink K, Shao H, Shao HB, Sun F, Sun YY, Singh AK, Taron J, Walther M, Wang W, Watanabe N, Wu N, Xie M, Xu W, Zehner B (2012a) OpenGeoSys: an open-source initiative for numerical simulation of thermo-hydro-mechanical/chemical (THM/C) processes in porous media. Environ Earth Sci. doi:10.1007/s12665-012-1546-x

Kolditz O, Bauer S, Beyer C, Böttcher N, Dietrich P, Görke UJ, Kalbacher T, Park CH, Sauer U, Schütze C, Shao HB, Singh AK, Taron J, Wang W, Watanabe N (2012b) A systematic benchmarking approach for geologic CO_2 injection and storage. Environ Earth Sci. doi:10.1007/s12665-012-1656-5

Kühn M et al (2012) CLEAN: CO2 large-scale enhanced gas recovery in the Altmark natural gas field (Germany): project overview. Environ Earth Sci, submitted (this issue)

Li H, Li G (2010) Modeling surface heave induced by hydraulic fracturing stimulation and CO_2 injection into coal seams. In: 44th USA rock mechanics symposium and 5th USA–Canada rock mechanics symposium, SPE, 10-319

Martens S, Kempka T, Liebscher A, Lueth S, Moeller F, Myrttinen A, Norden B, Schmidt-Hattenberger C, Zimmer M, Kuehn M, Ketzin Group (2012) Europe's longest-operating on-shore CO_2 storage site at Ketzin, Germany: a progress report after three years of injection. Environ Earth Sci, this issue

Millington RJ, Quirk JM (1961) Permeability of porous solids. Trans Faraday Soc 57:1200–1207

Oldenburg CM (2003) Carbon sequestration in natural gas reservoirs: enhanced gas recovery and natural gas storage. In: Proceedings of TOUGH Symposium 2003, LBNL, Berkeley

Oldenburg CM, Moridis GJ, Spycher N, Pruess K (2004) EOS7C version 1.0: TOUGH2 module for carbon dioxide or nitrogen in natural gas (methane) reservoirs. Lawrence Berkeley National Laboratory, LBNL-56589

Ouellet A, Bérard T, Desroches J, Frykman P, Welsh P, Minton J, Pamukcu Y, Hurter S, Schmidt-Hattenberger C (2011) Reservoir geomechanics for assessing containment in CO_2 storage: a case study at Ketzin, Germany. In: 10th international conference on greenhouse gas control technologies (GHGT). Energy Procedia, 4:3298–3305

Park CH, Böttcher N, Wang W, Kolditz O (2011) Are upwind techniques in multi-phase flow models necessary? J Comp Phy 230(22):8304–8312. doi:10.1016/j.jcp.2011.07.030

Poling BE, Prausnitz JM, O'Connell JP (2001) The properties of gases and liquids, 5th edn. McGraw-Hill, New York

Quintella CM, Dino R, Musse APS (2010) CO_2 enhanced oil recovery and geologic storage: an overview with technology assessment based on patents and articles. In: SPE international conference on health, safety and environment in oil and gas exploration and production, SPE 126122-MS

Rutqvist J, Tsang CF (2002) A study of caprock hydromechanical changes associated with CO_2 injection into a brine aquifer. Environ Geol 42:296–305

Rutqvist J, Borgesson L, Chijimatsu M, Kobayashi A, Jing L, Nguyen TS, Noorishad J, Tsang C-F (2001) Thermohydromechanics of partially saturated geological media: governing equations and formulation of four finite element models. Int J Rock Mech Min Sci 38:105–127

Rutqvist J, Wu YS, Tsang CF, Bodvarsson G (2002) A modeling approach for analysis of coupled multiphase fluid flow, heat transfer, and deformation in fractured porous rock. Int J Rock Mech Min Sci 39:429–442

Rutqvist J, Barr D, Birkholzer JT, Chijimatsu M, Kolditz O, Liu Q, Oda Y, Wang W, Zhang C (2008) Results from an international simulation study on coupled thermal, hydrological, and mechanical processes near geological nuclear waste repositories. J Nucl Technol 163(1):101–109

Schütze C, Sauer U, Beyer K, Lamert H, Strauch G, Braeuer K, Flechsig C, Kaempf H, Dietrich P (2012) Natural analogues—a potential approach for developing reliable monitoring methods to understand subsurface CO_2 migration processes. Environ Earth Sci, submitted (this issue)

Sweatman R, Crookshank S, Edman S (2011) Outlook and technologies for offshore CO_2 EOR/CCS projects. In: Offshore technology conference, Houston, SPE 21984-MS

Taron J, Elsworth D, Min K-B (2009) Numerical simulation of thermal-hydrologic-mechanical-chemical processes in deformable, fractured porous media. Int J Rock Mech Min Sci 46(5):842–854. doi:10.1016/j.ijrmms.2009.01.008

Van der Meer LGH, Kreft E, Geel C, Hartman J (2005) K12-B: a test site for CO2 storage and enhanced gas recovery. In: Proceedings of the SPE Europec/EAGE annual conference, SPE 94128

Wang W, Rutqvist J, Goerke U-J, Birkholzer JT, Kolditz O (2011) Non-isothermal flow in low permeable porous media: a comparison of unsaturated and two-phase flow approaches. Environ Earth Sci 62(6):1197–1207. doi:10.1007/s12665-010-0608-1

Watanabe N, Wang W, Taron J, Goerke U-J, Kolditz O (2012) Lower-dimensional interface elements using local enrichments and application for a coupled hydromechanical problem in fractured rock. I J Numer Met Eng. doi:10.1002/nme.3353